

# CONTENTS

## VOLUME 2

Contents . . . . .	i
--------------------	---

### CHAPTER SEVEN

#### The Prediction of Non-Uniform Elongation

7.1 Introduction . . . . .	1
7.2 The Stress-Strain Curve . . . . .	2
7.3 The Factors Controlling Ductility . . . . .	4
7.4 Experimental Method . . . . .	7
7.5 Results . . . . .	8
7.6 Discussion . . . . .	11
7.7 Summary . . . . .	16
References . . . . .	18

### CHAPTER EIGHT

#### Weld Metal Ductility: Reduction in Area

8.1 Introduction . . . . .	20
8.2 Stress Intensification . . . . .	20
8.3 The Necking Process and Reduction in Area . . . . .	21
8.4 Models . . . . .	24
8.5 Discussion . . . . .	27
8.6 Summary . . . . .	29
References . . . . .	31

### CHAPTER NINE

#### Scatter in Weld Metal Toughness Measurements

9.1 Introduction . . . . .	34
9.2 Analysis of Scatter . . . . .	36
9.3 Quantification of Heterogeneity . . . . .	38
9.4 Results . . . . .	40
9.5 Discussion . . . . .	43
9.6 The Effect of Tempering on Weld Metal Hardness . . . . .	43
9.7 Summary . . . . .	45

References . . . . .	46
----------------------	----

## CHAPTER TEN

### The Discovery of Lower Acicular Ferrite

10.1 Introduction . . . . .	48
10.2 The Formation of Bainite . . . . .	49
10.3 Acicular Ferrite . . . . .	52
10.4 Experimental Method . . . . .	52
10.5 Results . . . . .	54
10.6 Discussion . . . . .	56
10.7 Summary . . . . .	57
References . . . . .	59

## CHAPTER ELEVEN

<u>A Programme for Future Research</u> . . . . .	61
References . . . . .	66

## APPENDICES

Appendix 1: Ae3 Program . . . . .	67
Appendix 2: Determination of $\Delta T$ . . . . .	77
Appendix 3: Peritectic Program . . . . .	82
Appendix 4: Strengthening Program . . . . .	97
Appendix 5: Strain-Hardening Coefficients Program . . . . .	114
Appendix 6: Heterogeneity Program . . . . .	117

# CHAPTER 7

## THE PREDICTION OF NON-UNIFORM ELONGATION

### 7.1 INTRODUCTION

The ductility of a metal is a measure of its ability to deform plastically without failure, and it is one of the most important parameters used to describe the mechanical behaviour of materials. In welding, it is conventional to specify minimum levels of required ductility for safe performance of the welded structure. Since the ability of a weldment to serve the purpose for which it was fabricated requires strict control of its mechanical properties, any systematic study of the factors which determine weld metal properties must include an investigation into the factors controlling their ductility. This work is of increased interest, since it was demonstrated in Chapter 5 how the true stress/true strain curve may be estimated for as-deposited microstructures up to the ultimate tensile strength.

The ductility of a specimen elongated in a tensile test is conventionally measured in two ways; from the engineering strain at fracture,  $\epsilon_f$ , (usually called the elongation), and the reduction in area at fracture, both usually expressed as a percentage. However, a major problem in analysing these two parameters, as Dieter (1976) pointed out, is that the occurrence of necking in the tension test makes any quantitative conversion between the two measures impossible. Separate treatments are, therefore, necessary.

The detailed characteristics of ductile failure in steel welds are a consequence of the presence of inclusions in the material which act as stress concentrators, and it is now recognized that the size distribution of inclusions in weld metals is an important factor in determining their properties (Cochrane and Kirkwood, 1979; Savage, 1980). Likewise, other details of the inclusion population are increasingly being highlighted as being influential on the mechanical properties of weld metals (Abson and Pargeter, 1986; Dowling *et al.*, 1986; Shehata *et al.*, 1987). It is expected, therefore, that the volume fraction of inclusions will be a critical parameter for ductility. However, in order to provide a general quantitative description of the ductile behaviour of weld metals, it will also be necessary to consider other

factors, such as the influence of the state of stress and strain in the material, and the work-hardening properties of the metal (Teirlinck *et al.*, 1988). This work aims to identify the main factors that influence the engineering properties of elongation and reduction in area in weld metals, and to provide models by which they may be predicted. Whilst a limited amount of work has been done on modelling the ductile failure of steel weld metals (Hill and Passoja, 1974; Farrar, 1976; Roberts *et al.*, 1982), research has concentrated on the properties of weld metals under impact, rather than under uniaxial tensile loading. This chapter, and the one following, aim to show that elongation and reduction in area are dependent upon different parameters, and describe different aspects of materials behaviour; simple models are presented to describe them.

## 7.2 THE STRESS-STRAIN CURVE

The engineering tension test is used widely as an experimental technique by which the mechanical properties of a material may be evaluated, and also as a standard test by which the quality of a material may be adjudged. It involves a specimen being subjected to a continually increasing uniaxial load, whilst simultaneously the elongation of the specimen is recorded. An engineering stress-strain curve can then be constructed from the load-elongation measurements made on the test specimen. The engineering stress is a measure of the average longitudinal stress in the tensile specimen, and is obtained by dividing the load at a given point by the original cross-sectional area of the specimen. Similarly, the engineering strain,  $e$ , is the average linear strain, and is obtained by dividing elongation of the initial gauge length of the specimen,  $\Delta l$ , by its original length,  $l_0$  (Dieter, 1976). This gives

$$e = \frac{\Delta l}{l_0} = \frac{l - l_0}{l_0} \quad (7.1)$$

where  $l$  is the gauge length.

Figure 7.1 shows a typical engineering stress-strain tensile test curve. In the elastic region up to the yield stress, stress is linearly related to strain by the Young's modulus. When the yield stress is exceeded the specimen undergoes gross plastic deformation. Then, as the metal work-hardens, the stress to produce continued plastic deformation increases with increasing strain, and the strain is accommo-

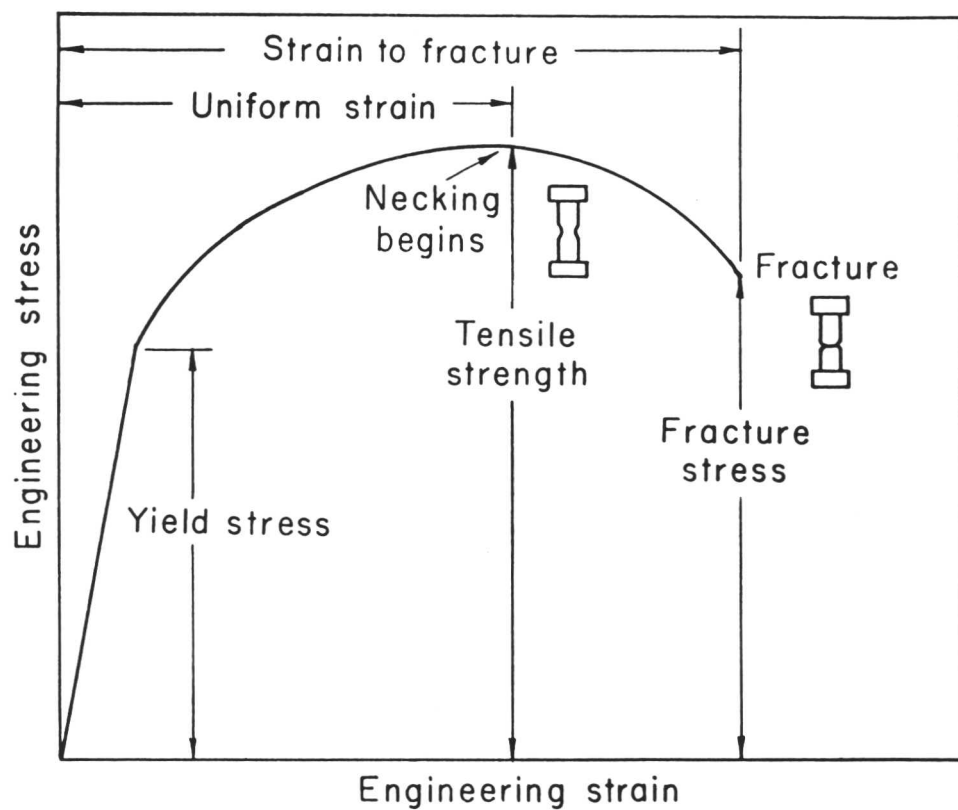


Figure 7.1: Engineering stress-strain curve. (After Dieter, G. E. (1968), Introduction to Ductility, in "Ductility", American Society for Metals, Chapman and Hall Ltd., London, U.K., 3).

dated uniformly throughout the specimen. During this period the volume remains essentially constant, and as the specimen lengthens it decreases uniformly across the gauge length in cross-sectional area. The flow curve of many metals in the region of uniform plastic deformation can be expressed empirically by the simple power law curve relation due to Nadai (1931):

$$\sigma = K\epsilon^n \quad (7.2)$$

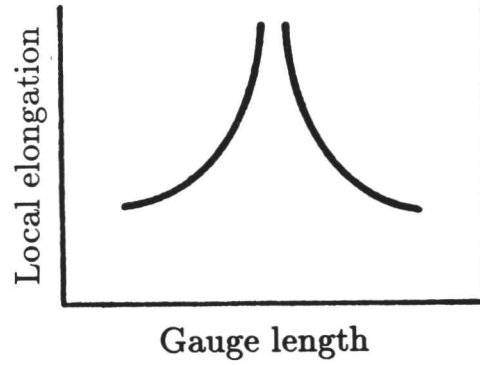
where  $\epsilon$  is the true strain

$n$  is the strain hardening exponent

and  $K$  is the strength coefficient, equal to the value of the flow stress at  $\epsilon^n = 1.0$ .

This equation describes a state of stable yielding, and, although a number of alternative equations exist, it is this equation which has been most successfully applied by various workers in describing weld metal tensile behaviour in this regime (Tweed, 1983; McRobie and Knott, 1985).

Eventually a point is reached where the decrease in area is greater than can be supported by the increase in deformation load arising from strain hardening. The maximum stress associated with this point is the ultimate tensile strength,  $\sigma_{UTS}$ , and the strain at maximum load up to which the cross-sectional area decreases uniformly along the gauge length, is the uniform elongation,  $\epsilon_u$ . Following the UTS, an instability will be reached at a point in the specimen that is slightly weaker than the rest. Further plastic deformation is concentrated in this region, and the specimen begins to neck down locally. The onset of necking may be defined by the Considère construction (Considère, 1885). Plastic deformation during necking is confined to the necked region, and the applied load continues to drop until the specimen fractures. This is illustrated in Figure 7.2. For steels, beyond necking, the true stress-strain curve is almost linear to fracture (Le Roy *et al.*, 1981). It is important to observe that once necking occurs, the constraints produced by the non-deforming region outside the neck produce a state of triaxial stress in the neck. Thus, the average stress required to cause flow from maximum load to fracture is higher than would be required if only uniaxial stress were present. Eventually the specimen fails by strain under conditions approaching plane strain to give the cone part of a typical 'cup and cone' fracture (Rogers, 1960; Bluhm and Morrissey, 1966).



---

Figure 7.2: Variation of local elongation with position along the gauge length of a tensile specimen. (After Dodd, B., and Bai, Y. (1987), "Ductile Fracture and Ductility", Academic Press Inc. Ltd., London, U.K., 28.)

This fracture effectively takes place by internal necking of the matrix material.

The true strain during testing is defined as follows:

$$\epsilon_L = \ln \left( \frac{l}{l_0} \right) \quad (7.3)$$

---

In this work, the subscripts L and A will be used to differentiate explicitly between strain calculated from change in length, and strain calculated from change in cross-sectional area respectively.

---

This equation is only applicable to the onset of necking while there is a homogeneous distribution of strain along the gauge length of the tensile specimen. Beyond maximum load, the true strain should be based on measurements of the actual area (A) or diameter (D), when

$$\begin{aligned} \epsilon_A &= \ln \left( \frac{A_0}{A} \right) \\ &= 2 \ln \left( \frac{D_0}{D} \right) \end{aligned} \quad (7.4)$$

### 7.3 THE FACTORS CONTROLLING DUCTILITY

Ductile failure commonly occurs progressively, with void or crack nucleation at inclusions or particles, the growth of these voids with increasing plastic strain, and finally coalescence of the voids. Thus, it follows that the presence of particles in the microstructure can markedly affect ductility. Void coalescence occurs in the centre of the specimen. The central crack grows rapidly to complete fracture by the continued linking of voids as the applied load is accommodated by steadily fewer ligaments of matrix. Final separation occurs as the result of intense shear between voids.

Any discontinuity such as an inclusion in a material will cause a disturbance of a uniform applied stress field. Having nucleated voids or particles, the holes then

---

Shape of Specimen	Cylindrical Sheet Other
Particles	Volume fraction
Type of particle	Inclusion Precipitate Dispersion
Particle shape	Spherical Elongated
Particle size	<10 nm; 0.05-1 $\mu$ m; > 1 $\mu$ m
Particle location	Matrix Grain boundary Spacing between particles Orientation
Grain structure of matrix	Size Shape Preferred orientation Grain boundaries
Free surface energy	Matrix Particle Matrix-particle
State of stress	Uniaxial Triaxial Hydrostatic Normal stress
Strain	Magnitude Rate
Stress	Yield stress Flow stress Fracture stress
Strain hardening	Dislocation cell structure Deformation mode due to stacking fault energy

---

Table 7.1: Variables in fracture mechanisms involving second-phase particles. (After H. G. F. Wilsdorf, *Mat. Sci. Eng.*, (1983), 59, 32).

grow as the applied tensile strain increases until they coalesce to give a fracture path (Fig. 7.3). Because of its stress-concentrating effect, a spherical void will elongate initially at a rate of about twice that of the specimen itself. As it extends and becomes ellipsoidal, however, it grows more slowly until, when very elongated, it extends at the same rate as the specimen itself (Martin, 1980).

Criteria for ductile fracture must take into account the fact that these different processes are involved and the parameters controlling them. The factors that can affect the ductility of a given material are given in Table 7.1 overleaf. The main variables are yield stress and the work hardening rate of the matrix, the cohesion of the matrix/particle interface, the size and shape of the second phase particles, their hardness, their volume fraction and their number per unit volume. Inevitably, in such a complicated situation, criteria for ductile fracture give weight to only a few of these factors, and will tend, therefore, to be applicable only to certain situations, but experience suggests that the work-hardening characteristics of the matrix material, and the nature of the inclusion population are the main causal factors in determining the true strain experienced during non-uniform deformation.

Percent elongation is primarily dependent upon the physico-mechanical properties of the material, and will be a function of the capacity of the material to work-harden. However, a complication in modelling elongation is that, since an appreciable fraction of the deformation will be concentrated in the necked region of the specimen, the value of  $e_f$ , the final total strain, will depend on the gauge length,  $l_o$ , over which the measurement is taken. The smaller the value of  $l_o$ , over which the measurement is taken, the greater the contribution from the neck and the higher the value of  $e_f$ . This gauge length dependence must also be accounted for. In fact, because percent elongation and percent reduction in area are both dependent upon specimen geometry and deformation behaviour they should not be taken unreservedly as true material properties. Nevertheless, they are valuable, widely used, guides to ductility, and useful in detecting quality changes in weld metals.

The factors that control the observed values for reduction in area are discussed in detail in Chapter 8.

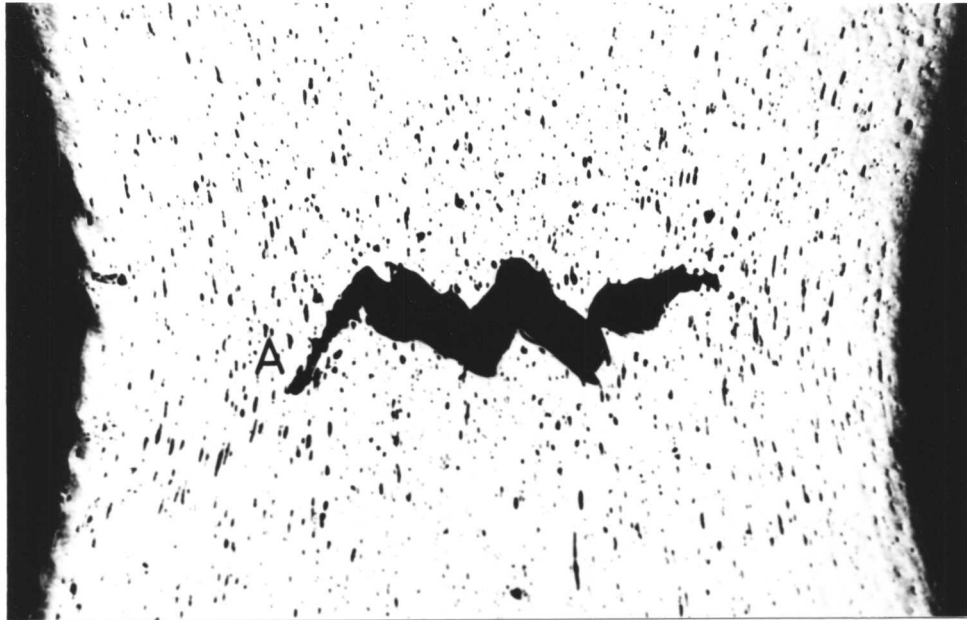


Figure 7.3: Macroscopic central cavity formed in neck of copper tensile specimen immediately prior to fracture. The final shear stage of separation has started (at A). (After Groom, J. D. G. (1971), Ph.D. thesis, University of Cambridge, U.K., Chapter 1).

## 7.4 EXPERIMENTAL METHOD

An experiment was designed in order to see how ductility varies for weld metal with the same composition, and inclusion population, but with different matrix strengths. To do this, tensile testing was carried out on a series of welds at a variety of temperatures, so that different strengths would be exhibited.

Five low-carbon manganese multipass welds were fabricated to give welds of approximately constant chemical composition. The joint geometry was in accordance with ISO 2560-1973 specifications. The number of weld runs was 23 or more, with three runs deposited per layer. The current and voltage used were 180A and 23V (DC positive) respectively. The net heat input was approximately 1.5 kJ/mm, and the maximum interpass temperature was 250°C. The nominal plate and deposit composition were Fe-0.12C-0.55Mn-0.25Si wt%, and Fe-0.07C-1.2Mn-0.05Si wt% respectively. The number of beads per weld was usually 25, and not less than 23. The weld metal compositions are given in Table 7.2.

Weld No.	Composition /wt%											ppm	
	C	Mn	Si	P	S	Cr	Ni	Mo	V	Ti	Al	N	O
7.1	0.058	1.28	0.44	0.019	0.008	0.05	0.05	0.01	0.008	0.009	0.005	85	316
7.2	0.060	1.31	0.44	0.018	0.008	0.06	0.06	0.01	0.006	0.008	0.014	97	352
7.3	0.054	1.33	0.45	0.017	0.008	0.03	0.03	0.01	0.002	0.008	0.004	79	293
7.4	0.053	1.30	0.44	0.018	0.008	0.02	0.03	0.01	0.003	0.008	0.003	92	305
7.5	0.056	1.36	0.46	0.018	0.008	0.03	0.03	0.01	0.005	0.008	0.004	85	345

Table 7.2: Weld metal analyses.

Two *all-weld* metal tensile specimens, threaded at each end, with cylindrical gauge lengths were extracted longitudinally and machined from each weld in accordance with SMS 674-10C50 specifications to give five pairs of tensile specimens in all, although, because of the limited amount of weld metal available, four of the specimens could only be made with a gauge length of 55mm instead of the recommended 70mm. The specimens were degassed for 16 hours at 250°C to remove hydrogen prior to testing. By testing at more than one temperature, this work would also complement the work described in Chapter 5 when a computer program was written depicting the effect of temperature on the strength of iron

and solid solution strengthening of alloying elements in iron.

Tensile testing was carried out *in situ* at ambient temperature, 0, -20, -40 and -60°C, the temperatures being achieved using mixtures of dry-ice and alcohol. The strain rate was approximately  $2 \times 10^{-4}$ /s. The tensile specimens were threaded into place, and then a Pt thermocouple was taped to each specimen prior to testing to ensure that the appropriate temperature was attained, although during testing the temperature recorded unavoidably rose an average of 8.5°C as a consequence of deformation-induced heat evolution.

## 7.5 RESULTS

Tensile testing results are given in Table 7.3.  $\sigma_y$  is the yield strength, and  $\sigma_{UTS}$  is the ultimate tensile strength. The elongation and reduction in area at fracture have been designated EL and q respectively. Figure 7.4 shows that tensile failure occurred by a ductile 'cup and cone' mechanism.

Weld No.	T/K	$\sigma_y$ /MPa	$\sigma_{UTS}$ /MPa	$\sigma_y/\sigma_{UTS}$	EL (%)		q (%)
					on 70mm	on 55mm	
7.1A	297	522	561	0.930	–	26.8	76
7.1B	296.5	512	550	0.931	28.8	–	76
7.2A	273	506	571	0.886	25.4	–	75
7.2B	273	528	566	0.933	–	27.8	76
7.3A	253	536	586	0.915	27.6	–	75
7.3B	253	535	586	0.913	29.6	–	75
7.4A	233	511	599	0.853	29.6	–	75
7.4B	233	533	608	0.877	–	29.9	75
7.5A	213	567	619	0.916	29.6	–	75
7.5B	213	571	619	0.922	–	30.8	76

Table 7.3: Welds 1–5: Results for mechanical testing results, carried out at temperature T.

During tensile testing, plastic deformation will be accommodated in the tensile

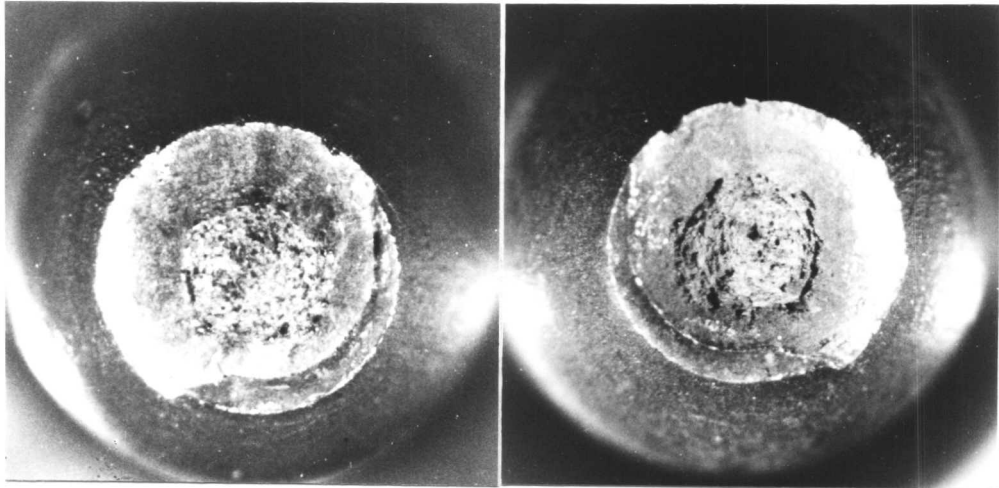


Figure 7.4: End-on view of the two halves of a tensile test specimen (Weld 1A) showing 'cup and cone' fracture ( $\times 15$ ).

specimen. Elastic extension, however, will occur in both the specimen and the tensile testing machine, thus making the actual elongation, as determined from load-extension curves, appear larger than it actually is. This behaviour can lead to errors in estimates of Young's modulus of up to 2 orders in magnitude (Thompson, 1988). It was found that elastic stretching of the machine caused the gradient of the elastic line on the stress-strain curves, which should have a value of the modulus of elasticity for the material, to be only  $\frac{1}{10}$  of its expected value. Accordingly, the components of elastic strain and plastic strain,  $\epsilon_e$  and  $\epsilon_p$ , were calculated separately.

The elastic extension,  $\Delta l_e$ , has been calculated from Young's modulus,  $E$ . The modulus of elasticity for a material, as determined at ambient temperature, is extremely structure insensitive, and only slightly affected by changes in composition. For low-alloy steel weld metal,  $E \approx 207\text{GPa}$  (Dieter, 1976). Therefore, from the definition of Young's modulus

$$\Delta l_e = \frac{\sigma l_0}{E} \quad (7.5)$$

*Note that this depends on strain being an engineering strain*

where  $\sigma$  is the average stress on the material.

Therefore

$$\Delta l_e = \frac{F}{E} \times \frac{l_0}{A} \quad (7.6)$$

where  $F$  is the applied load.

$A$  has been calculated as follows. Since the reduction in area before the UTS is reached occurs uniformly along the specimen then, at any given time, assuming constant volume,

$$\begin{aligned} A_0 l_0 &= A l \\ &= A(l_0 + \Delta l_p + \Delta l_e) \end{aligned}$$

for which  $\Delta l_p$  is the plastic extension of the specimen.

Therefore

$$\frac{l_o}{A} = \frac{1}{A_o}(l_o + \Delta l_p + \Delta l_e) \quad (7.7)$$

It follows, from Eqn. 7.6,

$$\Delta l_e = \frac{F}{EA_o}(l_o + \Delta l_p + \Delta l_e) \quad (7.8)$$

Therefore

$$\Delta l_e EA_o - F\Delta l_e = F(l_o + \Delta l_p)$$

which leads to

$$\Delta l_e = \frac{F(l_o + \Delta l_p)}{EA_o - F} \quad (7.9)$$

The extension due to plastic deformation,  $\Delta l_p$ , is read directly from the load-extension curve, as shown in Figure 7.5. The elastic and plastic elongations, and plastic strain experienced by the specimens during tensile testing are given in Table 7.4.  $F_{UTS}$  is the applied load at the UTS,  $\Delta l_{u_e}$  and  $\Delta l_{u_p}$  are the elastic and plastic extensions achieved during *uniform* elongation,  $\Delta l_{u_{Total}}$  is the total uniform elongation, and  $\epsilon_{u_p}$  is the value of the uniform plastic strain for the welds tested.

The total uniform plastic strain,  $\epsilon_{u_p}$ , corresponds, therefore, to the total strain up to the ultimate tensile strength, since the elastic component is relieved at fracture.

Although elongation varied with temperature, Figures 7.6a and b show that for the temperature range investigated, reduction in area did not change.†

---

† It would be misleading to try to relate percent elongation and temperature from the data recorded, since elongation is a function of gauge length and the specimens used were not of identical geometry.

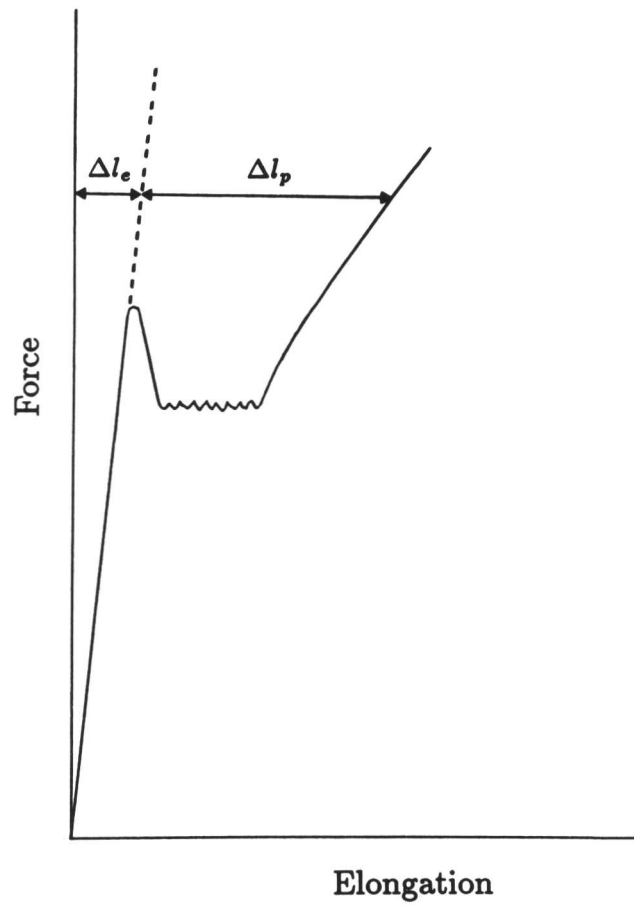


Figure 7.5: Illustrating the distinction between the elastic and plastic components of a load-elongation curve.

Weld No.	$F_{UTS}$ kN	$l_o$ mm	$A_o$ mm <sup>2</sup>	$\Delta l_{u_e}$ mm	$\Delta l_{u_p}$ mm	$\Delta l_{u_{Total}}$ mm	$e_{u_p}$
7.1A	43.3	69	78.7	0.211	10.5	10.3	0.146
7.1B	43.5	55	78.4	0.170	8.09	8.26	0.147
7.2A	44.5	70	78.1	0.219	9.33	9.55	0.133
7.2B	44.8	52	78.4	0.167	8.66	7.83	0.167
7.3A	46.4	73	78.5	0.240	10.9	11.1	0.149
7.3B	46.1	71	78.5	0.232	10.7	10.9	0.151
7.4A	48.1	71	78.5	0.243	12.5	12.7	0.177
7.4B	47.1	54	78.4	0.189	9.64	9.83	0.178
7.5A	47.6	70	78.5	0.247	12.4	12.6	0.177
7.5B	47.4	64	78.4	0.223	10.5	10.7	0.164

Table 7.4: Calculation of plastic strain for Welds 7.1–7.5.

## 7.6 DISCUSSION

The extension of a specimen at fracture can be expressed according to the expression due to Barba (1880):

$$l_f - l_o = \alpha + e_{u_L} l_o \quad (7.10)$$

where  $l_f$  is the final gauge length of the specimen,

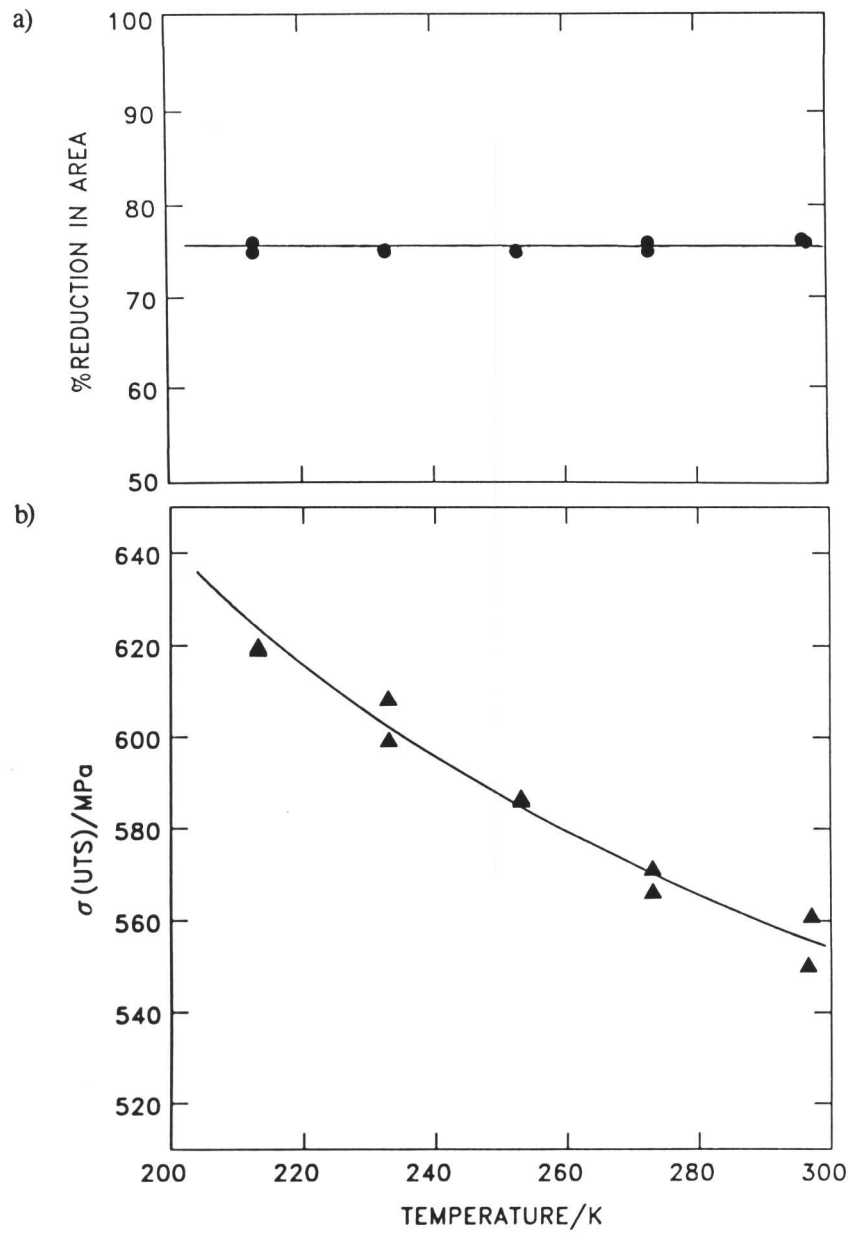
$\alpha$  is the local necking extension,

and  $e_{u_L} l_o$  is the uniform extension of the specimen.

This gives

$$e_f = \frac{\alpha}{l_o} + e_{u_L} \quad (7.11)$$

The local necking extension,  $\alpha = \beta\sqrt{A_o}$ . Therefore, from Barba's law, the



Figures 7.6a and b: (a) Reduction in area, and (b) ultimate tensile strength as a function of temperature for the experimental welds.

elongation:

$$e_{fL} = \beta \frac{\sqrt{A_o}}{l_o} + e_{uL} \quad (7.12)$$

where  $\beta$  is a constant of proportionality (Unwin, 1903).

Although  $\beta$  is taken as constant in a weld metal, it could be expected to be a function of the inclusion content, and so, indirectly, the amount of oxygen, sulphur, &c. , in the weld, since the extent of non-uniform deformation must depend on these factors.

Eqn. 7.12 clearly shows that the total elongation is a function of the specimen gauge length, and, therefore, to compare elongation measurements of different sized specimens the specimens must be geometrically similar, *i.e.* for round bars  $\frac{l_o}{D_o}$  should be fixed. In this analysis, data due to Widgery (1974; 1976) have been used. Widgery carried out mechanical tests on a large series of GMAW low-alloy steel welds. This work was particularly interesting because it included a detailed examination of the inclusion populations of 16 welds. More importantly, the maximum uniform strain achieved by each specimen in the course of tensile testing,  $\epsilon_u$ , was also recorded. Figure 7.7 shows the relationship between measured elongation,  $EL$ , and ultimate tensile strength,  $\sigma_{UTS}$ , for Widgery's welds. It can be seen that the recorded elongation decreases as the readiness of the weld metal to deform, as indicated by  $\sigma_{UTS}$ , increases.

$$\text{Since} \quad e_{uL} = \frac{l_u - l_o}{l_o}$$

$$\text{then} \quad \epsilon_{uL} = \ln(1 + e_{uL})$$

$$\text{and} \quad e_{uL} = \{\exp(\epsilon_{uL}) - 1\} \quad (7.13)^*$$

$$\text{Therefore \% Elongation} = e_{fL} \times 100$$

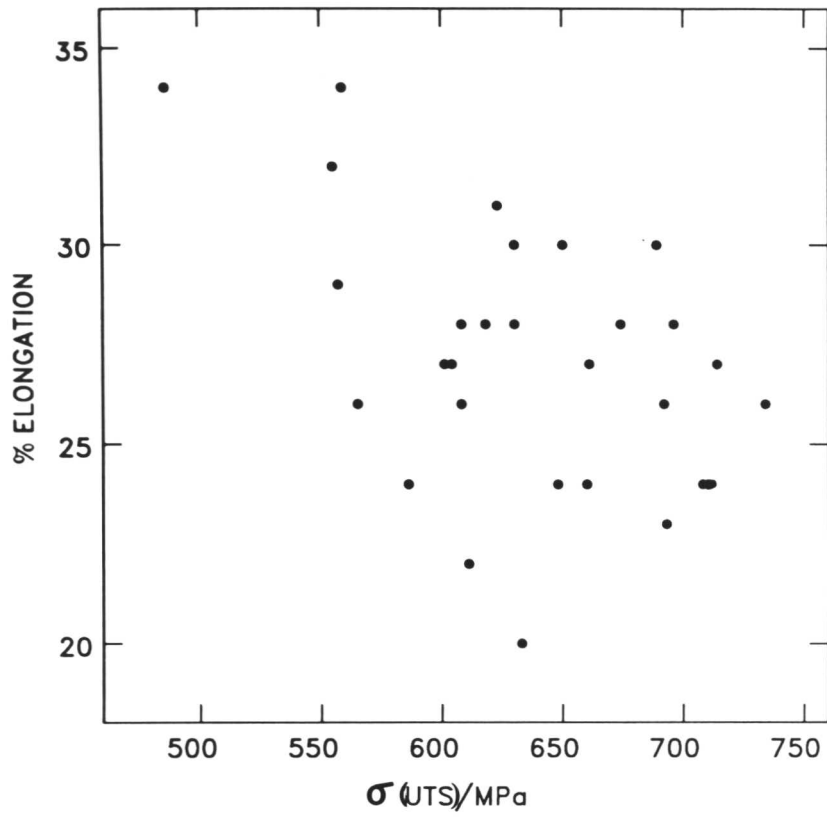


Figure 7.7: Showing the dependence of weld metal elongation on ultimate tensile strength. Data are due to Widgery (1976).

Check comparison

Weld No.	$\beta \frac{\sqrt{A_0}}{l_0}$	$\epsilon_{uLp}$ (Max)*	$\epsilon_{fL}$ (Calculated)	EL (%) (Measured)	EL (%) (Calculated)
7.1A	0.0937	0.146	0.242	26.8	24.2
7.1B	0.118	0.147	0.265	28.8	26.5
7.2A	0.0922	0.133	0.225	25.4	22.5
7.2B	0.124	0.167	0.291	28.8	29.1
7.3A	0.0886	0.149	0.238	27.6	23.8
7.3B	0.0911	0.151	0.242	29.6	24.2
7.4A	0.0911	0.177	0.268	29.6	26.8
7.4B	0.120	0.178	0.299	29.9	29.9
7.5A	0.0924	0.177	0.269	29.6	26.9
7.5B	0.101	0.164	0.265	30.8	26.5

\* Maximum uniform plastic strain.

Table 7.5: Measured and calculated values of percent elongation for the weld metal tensile specimens.

$$= \left\{ \beta \frac{\sqrt{A_0}}{l_0} + \exp(\epsilon_{uL}) - 1 \right\} \times 100 \quad (7.14)$$

It should be emphasized that  $\epsilon_{uL}$  is expected to be very closely related to the work-hardening coefficient,  $n$  (see *e.g.* Davies, 1978). Widgery (1974) found the two to be heavily correlated, with the best fit line:  $n = 0.024 + 0.65\epsilon_{uL}$ .  $\beta$  is dependent upon alloy microstructure and composition, but for low-alloy steels,  $\beta$  has a characteristic value of 0.73 (Lessels, 1954), and this was the value taken for the moment.

Figure 7.8 plots calculated and measured values of percent elongation for the experimental welds using data from Table 7.5. For Widgery's experiments, subsize specimens were used, but of recommended British standard dimensions (Lessels, 1954). The diameter and length were 8.41mm and 22.7mm respectively, ( $\frac{l_0}{D_0} =$

\* Engineering strain,  $e$ , and true strain,  $\epsilon$ , are essentially identical for strains less than 0.1, but for higher strains  $\epsilon$  is less than  $e$ .

10  
28

Check comparison line work

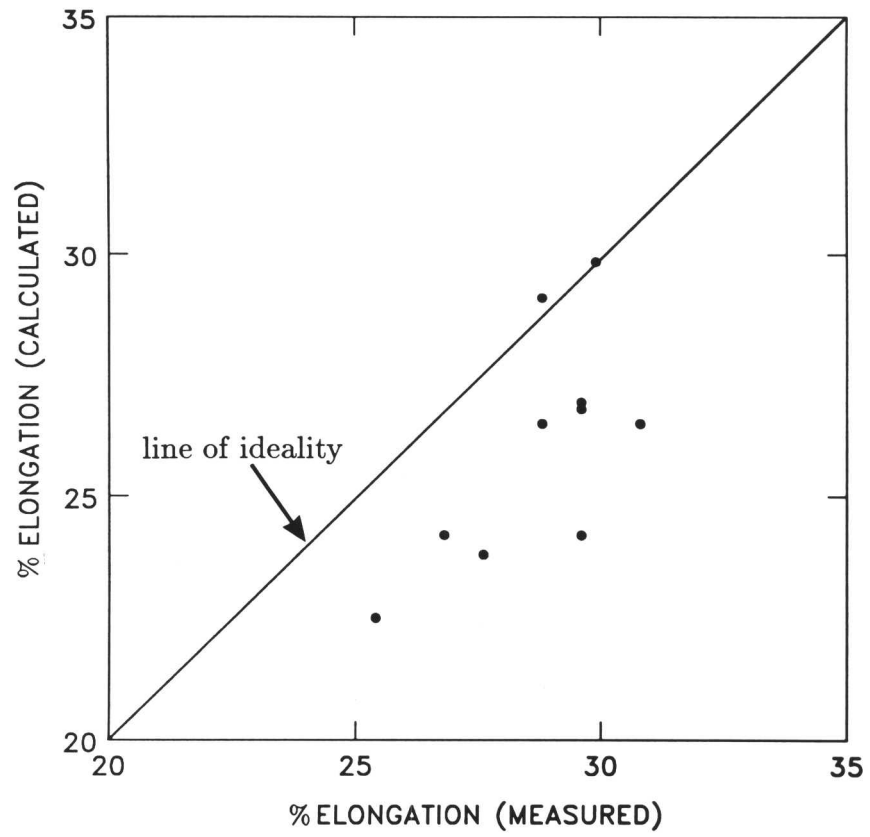


Figure 7.8: Calculated and measured values of percent elongation for the experimental welds (see Table 7.5).

3.54).

Table 7.6 lists the maximum uniform strain achieved, together with measured and calculated values for elongation, EL, and reduction in area at fracture, q. Figure 7.9 plots calculated and measured values of percent elongation for Widgery's welds. The fair agreement between theory and experiment implies the necking process contributes a fixed amount to the elongation. However, it can be seen that the graph does not concur with the data in Figure 7.8, even though both sets of data are internally consistent. The explanation for this is that  $\beta = 0.73$  applies to low-alloy *wrought* steels. However, because weld metals contain inclusions, not only will  $\beta$  tend to be smaller (since the amount of elongation by the specimen after the UTS will be reduced), but the value of  $\beta$  should correlate with the volume fraction of inclusions. The inclusion fraction, I, in volume %, may be evaluated using the approximate relationship (Widgery, 1977; Abson *et al.*, 1978; Widgery, 1979):

$$I \approx 5.5(\text{wt}\%[\text{O}] + \text{wt}\%[\text{S}]) \quad (7.15)$$

The best value for  $\beta$  was found to be

$$\begin{aligned} \beta &= 1.239 - 1.704 \times I \\ &= 1.239 - 9.372 \times (\text{wt}\%[\text{O}] + \text{wt}\%[\text{S}]) \end{aligned} \quad (7.16)$$

For example,  $I = 0.30$  vol% gives  $\beta = 0.73$ . However, for a larger volume fraction of 0.50 vol%,  $\beta$  drops to 0.39. Table 7.7 gives new calculated values for percent elongation incorporating Eqn. 7.16 to give

$$\begin{aligned} \% \text{Elongation} &= \{1.239 - 9.372 \times (\text{wt}\%[\text{O}] + \text{wt}\%[\text{S}])\} \\ &\quad \times \frac{\sqrt{A_o}}{L_o} + \exp(\epsilon_{uL}) - 1 \times 100 \end{aligned} \quad (7.17)$$

Calculated and measured values of percent elongation, EL, are plotted in Figure 7.10 for the experimental welds and for the data due to Widgery (1976). It

Weld	Maximum uniform strain, $\epsilon_u$	EL (%) (Measured)	EL (%) (Calculated)
A	0.115	26	30
B	0.105	24	29
C	0.10	24	29
D	0.13	28	32
E	0.10	23	29
F	0.095	22	28
G	0.09	20	28
H	0.11	24	30
J1	0.10	27	29
J2	0.12	28	31
J1R	0.11	24	30
J2R	0.13	27	32
J2RR	0.12	28	31
K	0.10	26	29
L	0.13	34	32
M	0.12	34	31
N	0.115	32	30
O	0.135	30	33
P	0.105	28	29
Q	0.07	24	24
R	0.115	30	30
S	0.11	26	30
T	0.125	29	32
U	0.12	27	31
W	0.08	24	27
X	0.13	30	32
Y	0.10	26	29
Z	0.13	31	32
Comm1	0.11	28	30
Comm2	0.10	27	29

Table 7.6: Calculation of percent elongation. (Welds given in Widgery (1976)).

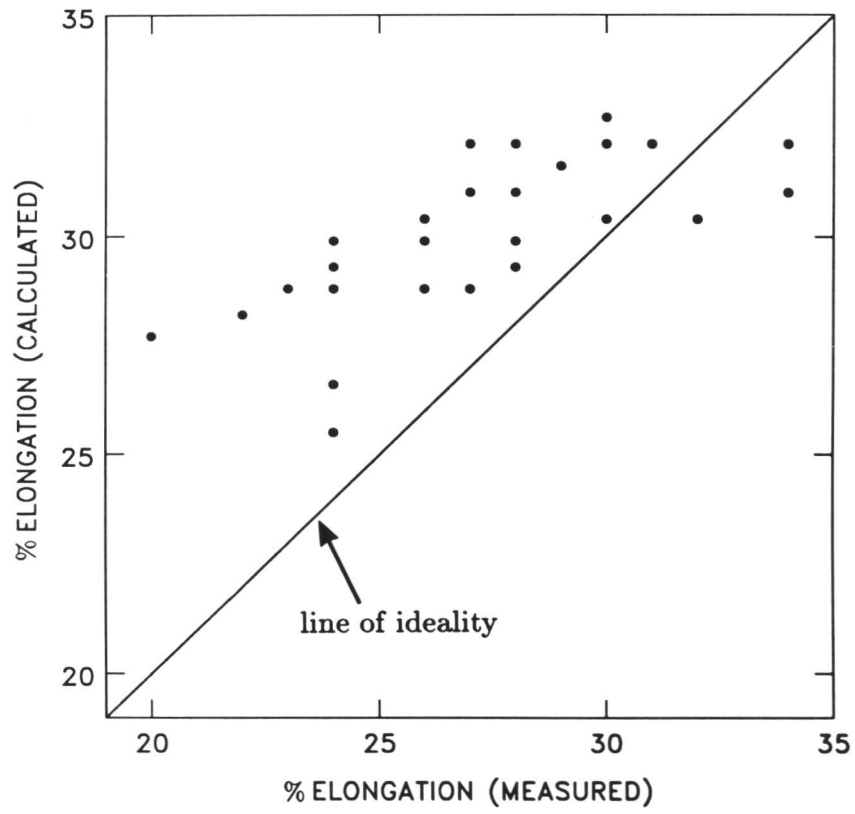


Figure 7.9: Measured elongations for 30 welds plotted against elongations calculated using Equation 7.16.

can be seen that the differences in gradient observed in Figures 7.8 and 7.9 have disappeared, and that general agreement is much better.

## 7.7 SUMMARY

The factors that control weld metal elongation have been reviewed. Up to necking, deformation occurs evenly along the length of the tensile specimen. For this region of the stress-strain curve, a strong correlation was observed between percent elongation and the maximum uniform strain,  $\epsilon_{uL}$ , which in turn is related directly to the work-hardening characteristics of the weld metal. Since it is already possible to estimate the uniform component of elongation for as-welded microstructures (see Chapter 5), an attempt to relate  $\epsilon_{uL}$  to the microstructure of multirun welds would be a suitable subject for future work, since this would then permit the prediction of weld metal strain to failure.

The strain experienced subsequent to necking is non-uniform, being dependent principally upon the inclusion size distribution, and volume fraction of inclusions in the weld deposit. It has been demonstrated that differences in measured elongation between sets of data for welds with known uniform elongations can be resolved in terms of differences in the volume fraction of inclusions in the weld metals, since they will influence the amount of local necking extension. A simple relationship has been arrived at, to allow the magnitude of this non-uniform contribution to be estimated for a given weld metal composition.

It has been found that the elongation of a weld metal tensile specimen can be predicted from a knowledge of the amount of the uniform elongation experienced during testing, (*i.e.* elongation up to the ultimate tensile strength), the chemical composition of the weld, and its geometry. This is done using a modified version of Barba's law, when the two components of uniform and non-uniform lengthening are treated separately.

The strength of the matrix, for the range considered, has no influence on reduction in area which is predicted to depend heavily upon the characteristics of the inclusion population.

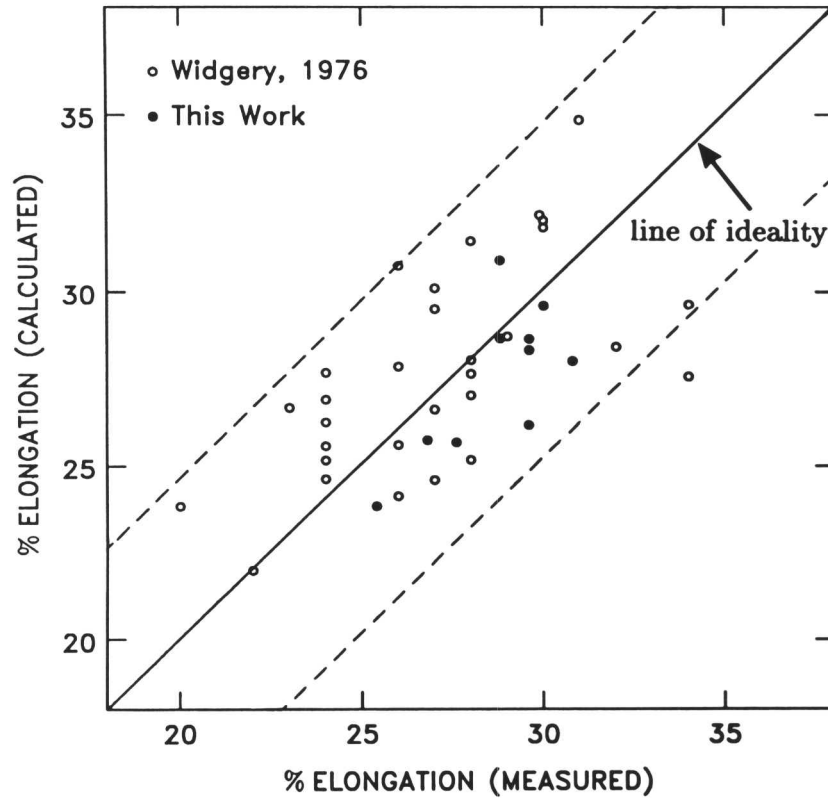


Figure 7.10: Recalculated and measured values for percent elongation for this work and for Widgery (1976), taking into account the inclusion population. The line of ideality, and 95% confidence limits are also drawn.

## REFERENCES

- ABSON, D. J., DOLBY, R. E., and HART, P. M. E. (1978), "Trends in Steels and Consumables for Welding", [*Proc. Conf.*], Welding Institute, Abington, U.K., 75-101.
- ABSON, D. J. and PARGETER, R. J. (1986), *Int. Met. Revs.*, **31**, (4), 141-194.
- BARBA, J. (1880), *Mem. Soc. Ing. Civ.*, (1), 682-710.
- BLUHM, J. I. and MORRISSEY, R. J., (1966) Proceedings of the First International Conference on Fracture, T. Yokobori, T. Kawasaki, and J. L. Swedlow, Eds., Japanese Society for Strength and Fracture of Materials, Japan, **3**, 1739-1780.
- COCHRANE, R. C. and KIRKWOOD, P. R. (1979), "Trends in Steels and Consumables for Welding", [*Proc. Conf.*], Welding Institute, Abington, U.K., 103-122.
- CONSIDERE, A., (1885) *Ann. Pont. et Chaussées*, **9**, 6, 574-775.
- DAVIES, R. G. (1978), *Metall. Trans. A*, **9A**, 451-455.
- DIETER, G. E. (1968), Introduction to Ductility, in "Ductility", American Society for Metals, Chapman and Hall Ltd., London, U.K., 1-30.
- DIETER, G. E. (1976), "Mechanical Metallurgy", 2nd Ed., McGraw-Hill, New York, 329-348.
- DODD, Brian and BAI, Yilong (1987), "Ductile Fracture and Ductility", Academic Press Inc. Ltd., London, U.K.
- DOWLING, J. M., CORBETT, J. M. and KERR, H. W. (1986), "Residuals in Steels", [*Proc. Conf.*], Welding Institute, Abington, U.K., 469-486.
- FARRAR, R. A. (1976), *Weld. Met. Fab.*, **44**, (10), 578-581.
- GROOM, J. D. G. (1971), Ph.D. thesis, University of Cambridge, U.K., Chapter 1.
- HILL, D. C. and PASSOJA, D. E. (1974), *Weld. J.*, **53**, (11), 481s-485s.
- LE ROY, G., EMBURY, J. D., EDWARDS, G., and ASHBY, M. F. (1981), *Acta Metall.*, **29**, 1509-1522.
- LESSELS, John M. (1954), "Strength and Resistance of Metals", John Wiley and Sons, Inc., New York, 71.
- MARTIN, J. W. (1980), "Micromechanisms in Particle-Hardened Alloys", Cambridge University Press, Cambridge, U.K., 110.

- McROBIE, D. E. and KNOTT, J. F. (1985), *Mat. Sci. Tech.*, **1**, (5), 357-365.
- NADAI, A., (1931) "Plasticity", McGraw-Hill Book Co., New York.
- ROBERTS, W., AHLBLOM, B., and HANNERZ, N.-E. (1982), "Advances in the Physical Metallurgy and Applications of Steels, [*Proc. Conf.*], 162-177.
- SAVAGE, Warren F. (1980), *Weld. World*, **18**, (5), 89-114.
- SHEHATA, M. T., CHANDEL, R. S., BRAID, J. E. M., and McGRATH, J. T. (1987), "Microstructural Science", Eds. Louthan, Jr., M. R., Le May, I., and Vander Voort, G. F., **14**, 65-76.
- TEIRLINCK, D., ZOK, F., EMBURY, J. D., and ASHBY, M. F. (1988), *Acta Metall.*, **36**, (5), 1213-1228.
- THOMPSON, H. (1988), Unpublished Research, University of Cambridge, U.K.
- TWEED, J. H. (1983) , Ph.D. thesis, University of Cambridge, U.K.
- TWEED, J. H. and KNOTT, J. F. (1983), *Metal Sci.*, **17**, (2), 45-54.
- UNWIN, W. C. (1903), *Proc. Inst. Civ. Eng.*, **55**, 170-233. (Discussion: 234-292).
- WIDGERY, D. J. (1974), Ph.D. thesis, University of Cambridge, U.K.
- WIDGERY, D. J. (1976), *Weld. J.*, **55**, (3), *Weld. Res. Supp.*, 57s-68s.
- WIDGERY, D. J. (1977), 'Factors controlling fracture by microvoid coalescence in as-deposited weld metals', Welding Institute Seminar, "The Toughness of Weld Metals", Newcastle-upon-Tyne, U.K., October 1977.
- WIDGERY, D. J. (1979), "Trends in Steels and Consumables for Welding", [*Proc. Conf.*], Welding Institute, Abington, U.K., 217-230.

Weld No.	[O] (wt%)	[S] (wt%)	$\epsilon_{uL}$	$\epsilon_{fL}$	EL (%) (Measured)	EL (%) (Calculated)
7.1A	0.032	0.008	0.146	0.268	26.8	25.8
7.1B	0.032	0.008	0.147	0.288	28.8	27.7
7.2A	0.035	0.008	0.133	0.254	25.4	23.8
7.2B	0.035	0.008	0.167	0.288	28.8	30.9
7.3A	0.029	0.008	0.149	0.276	27.6	25.7
7.3B	0.029	0.008	0.151	0.296	29.6	26.2
7.4A	0.031	0.008	0.177	0.296	29.6	28.7
7.4B	0.031	0.008	0.178	0.299	29.9	32.2
7.5A	0.034	0.008	0.177	0.296	29.6	28.3
7.5B	0.034	0.008	0.164	0.308	30.8	28.0
A	0.055	0.017	0.115	0.26	26.0	25.6
B	0.055	0.017	0.105	0.24	24.0	24.6
C	0.048	0.012	0.100	0.24	24.0	26.9
D	0.055	0.013	0.130	0.28	28.0	28.1
E	0.047	0.014	0.100	0.23	23.0	26.7
F	0.067	0.012	0.095	0.22	22.0	22.0
G	0.058	0.011	0.09	0.20	20.0	23.8
H	0.057	0.013	0.11	0.24	24.0	25.6
J1	0.060	0.010	0.10	0.27	27.0	24.6
J2	0.056	0.012	0.12	0.28	28.0	27.1
J1R	0.054	0.007	0.11	0.24	24.0	27.7
J2R	0.063	0.011	0.13	0.27	27.0	26.7
J2RR	0.063	0.013	0.12	0.28	28.0	25.2
K	0.064	0.008	0.10	0.26	26.0	24.1
L	0.063	0.007	0.13	0.34	34.0	27.6
M	0.048	0.009	0.12	0.34	34.0	29.6
N	0.053	0.007	0.115	0.32	32.0	28.4
O	0.045	0.009	0.135	0.30	30.0	31.8
P	0.048	0.011	0.105	0.28	28.0	27.7
Q	0.042	0.008	0.07	0.24	24.0	26.3
R	0.047	0.008	0.115	0.30	30.0	29.6
S	0.040	0.008	0.11	0.26	26.0	30.7
T	0.052	0.011	0.125	0.29	29.0	28.7
U	0.043	0.012	0.12	0.27	27.0	30.1
W	0.049	0.010	0.08	0.24	24.0	25.2
X	0.041	0.010	0.13	0.30	30.0	32.0
Y	0.046	0.010	0.10	0.26	26.0	27.9
Z	0.029	0.013	0.10	0.31	31.0	34.9
Comm1	0.034	0.011	0.11	0.28	28.0	31.5
Comm2	0.036	0.013	0.13	0.27	27.0	29.5

Table 7.7: Recalculation of percent elongation for welds given in Tables 7.5 and 7.6.